Fission of ^{215}Fr studied with γ spectroscopic methods

K. Miernik,[1,*] A. Korgul,[1] W. Poklepa,[1] J. N. Wilson,[2] G. Charles,[2] S. Czajkowski,[3] P. Czyż,[1] A. Fijałkowska,[1] L. M. Fraile,[4] P. Garczyński,[1] K. Hauschild,[2] C. Hiver,[2] T. Kurtukian-Nieto,[3] M. Lebois,[2] M. Llanos,[4] A. Lopez-Martens,[2] K. M. Deby Treasa,[3] J. Ljungvall,[2] I. Matea,[2] J. Mielczarek,[1] J. R. Murias,[4,5] G. Pasqualato,[2] A. Skruch,[1] K. Solak,[1] K. Stoyachev,[2] and I. Tsekhanovich[3]

[1]*Faculty of Physics, University of Warsaw, 02-093 Warsaw, Poland*
[2]*Université Paris-Saclay, CNRS/IN2P3, IJC Laboratory, Orsay, France*
[3]*Université Bordeaux, CNRS, LP2I Bordeaux, UMR 5797, F-33170 Gradignan, France*
[4]*Grupo de Física Nuclear and IPARCOS, Universidad Complutense de Madrid, CEI Moncloa, 28040 Madrid, Spain*
[5]*TRIUMF, 4004 Wesbrook Mall, Vancouver, British Columbia V6T 2A3, Canada*

(Received 24 July 2023; accepted 2 November 2023; published 22 November 2023)

Background: Asymmetric fission is known to occur in two regions, the actinides and sublead, and is dependent on the fissioning system excitation energy. Experimental evidence in the sublead region show that this mode is surprisingly persistent with increasing energy and its origin is not fully understood.
Purpose: To experimentally study the fusion-fission reaction of ^{215}Fr at moderate excitation energy and determine previously unknown independent fission yields and other properties.
Method: The compound nucleus was formed in the reaction $^{18}\mathrm{O} + ^{197}\mathrm{Au}$. The prompt γ rays emitted during the reaction were measured with the high efficiency and high granularity ν-ball-2 spectrometer. Independent fission yields of even-even nuclei were determined by detecting triple-gamma cascades in the fission fragments.
Results: The observed yields, although dominated by a symmetric peak, show maxima for heavy fragment of $Z \approx 54$–56, which is consistent with the known results in the actinide region but unexpected for the nuclide of interest, and at the studied excitation energy.
Conclusions: The mode of asymmetric fission is present even at relatively high excitation energies in the system studied. This observation matches experimental findings in the sublead region, contrary to the actinides, and so far there is no well-developed explanation of this phenomenon.

DOI: 10.1103/PhysRevC.108.054608

I. INTRODUCTION

One of the commonly observed properties of fission, relevant to the understanding of this process, is the mass and charge distribution of fragments. During the process of fission, nuclei can travel along different paths on the potential energy landscape, which results basically in two general fission modes, symmetric and asymmetric. The path depends on the fissioning system itself, and to some degree, on the reaction entrance channel and excitation energy. One of the key experiments on this matter was performed by Schmidt *et al.* [1], which studied 70 systems in the astatine to uranium region via Coulomb-excitation induced fission. Symmetric modes were found for systems with $A < 226$, and asymmetric above that. Another important previous result was the observation of unexpected highly asymmetric fission of ^{180}Hg (after β decay) [2] which triggered a great interest in theoretical modeling, using various approaches from phenomenological through microscopic-macroscopic to fully microscopic models [3–11]. A remarkable fact is that most of them could reproduce the observed asymmetric mass split of ^{180}Hg, however without common agreement on the physical explanation for it.

Many models predict asymmetric modes for low excitation energies ($E^* < 20$ MeV), accessible in Coulomb excitation, or β-delayed induced fission, and argue that the driving microscopic effects are washed out at higher excitation energies [5,7,8,10,11] resulting in only the symmetric mode. However, recent experimental works [12,13], show that the asymmetric mode is clearly seen at moderately high excitation energies in the sublead region. It is quite remarkable that these systems preserve their asymmetry even for a relatively high excitation energies up to $E^* = 70$ MeV [12]. Similar phenomena were observed for multinucleon transfer induced fission on U/Th/Pu targets [14] up to 60 MeV excitation energy, but it was explained by a multichance fission mechanism, which has a much greater impact in the heavier systems. All together there is currently no unambiguous answer or theoretical consensus on the questions of how the fission proceeds, how it depends on excitation energy, whether the microscopic structure preserved, and to what excitation energies. As the same theoretical models or approaches are used for description of entire chart of nuclides, and applied in astrophysics or super-heavy elements production planning, it is crucial to stringently test their predictive powers beyond current experimental knowledge.

In this article we report results of an experimental study of the independent fission yields, and other characteristics,

*kmiernik@fuw.edu.pl

of ^{215}Fr, obtained in the ^{18}O + ^{197}Au reaction. Due to the very short half-life of 101(15) ns [15], this nuclide was not observed in systematic studies of electromagnetic-induced fission [1], covering francium isotopes with mass number 206–212, and 217–218. Although the present results, by nature of the reaction used for the production, probe the fission at much higher excitation energy, this partially fills in the gap in information about fission in this region.

II. EXPERIMENTAL SETUP

The experiment was performed at the ALTO facitily (IJC Laboratory in Orsay, France) during the campaign with the ν-ball-2 spectrometer, which is an upgraded version of the previous ν-ball setup [16–18]. The spectrometer included 24 HPGe Clovers, ten co-axial HPGe, and 14 $LaBr_3$(Ce) detectors of (12 cylindrical and two conical). The detectors of each type were arranged in rings—a ring of HPGe detectors, two rings of Clovers, and two rings of $LaBr_3$(Ce) detectors. All germanium detectors were equipped with BGO anti-Compton shields, as well as five of the $LaBr_3$(Ce) detectors. In the analysis, for various reasons, only 18 clovers and four coaxial Ge detectors were used, along with 12 $LaBr_3$ detectors. The efficiency of the HPGe detectors, including Compton suppression and addback, reached maximum of a 6% at 180 keV. At energies 662 and 1408 keV it was 3.7% and 2.3%, respectively. The relative uncertainty of the efficiency calibration was below 2% in the range 100–1500 keV, and up to 6% outside that range, for the energies studied.

A pulsed beam of $^{18}O^{7+}$ at the energy 111 MeV, with an average intensity of 0.5 nA (maximum 2 nA) impinged on a thick, 50 μm ^{197}Au target, with a repetition rate of 400 ns and a pulse width of approximately 2 ns. Data from all of the detectors were collected in triggerless mode by the FASTER digital electronics acquisition system [19] with independent registration of individual channels based only on a threshold condition. As a result a total of 16 TB of data were collected during one week of experiment, and all selection and processing of data was performed off-line.

The analysis was performed with codes written in the Julia programming language [20] using direct calls to the FASTER digital electronics [19] C-library for the raw data format interpretation. The data included the on-board calculated energy and precise time using the CFD method with the time bit resolution of 7.8 ps. The analysis steps included identification of the radiofrequency signal, the alignment of all channels based on the time differences compared to the reference detector with the best timing resolution [one of the conical $LaBr_3$(Ce) detectors], walk correction, and a Compton suppression and addback procedures applied to the Clover detectors and BGO shielding at common location. Individual detector hits were then grouped into 400 ns events, in accordance to the beam pulsation period, but due to the limited time resolution of the HPGe detectors the event started 50 ns before the beam pulse, and ended 350 ns after. One- and two-dimensional spectra such as γ-γ coincidence, γ time, or γ multiplicity were incremented at that point, and all events with multiplicity 3 and more [taking into account HPGe and $LaBr_3$(Ce) detectors] were saved to a preprocessed list-mode HDF5 file [21] including data on energy, time, and types of detectors involved. This data format allows for the dynamic γ-γ-γ gates that can use various energy and time conditions depending on the case. In total 1.1×10^{10} threefold coincidences were registered, including 2.2×10^9 prompt coincidences recorded by the HPGe detectors alone.

III. GENERAL DESCRIPTION OF THE REACTION

The ^{18}O + ^{197}Au reaction was previously studied from the point of view of the production of $^{208–211}$Fr isotopes via fusion evaporations [22]. In another experiment [23] the angular distribution of fission fragments was measured. Since the excitation functions were well described by HIVAP code [24], we performed calculations using the same input parameters as [22]. Our experiment used a thick target, with the beam completely stopped within. Due to rapidly decreasing fission cross section 90% of reactions of that type occurs within first 8 μm of the target, and 99% within 12 μm. At the same time, thick target reduces Doppler widening of the γ rays emitted from the fission fragments.

To calculate the compound nucleus (CN) excitation energy, we integrated the expected rates starting from the maximum energy of the beam (111 MeV) down to 0 MeV, including the stopping power [25], and calculating the reaction rate for each energy step. The weighted mean of energy for each reaction channel gives the effective excitation energy of the CN, at which the reaction occurs in the target. The most intense channels are total fission (47%), evaporation of five neutrons (5n) (^{210}Fr 22%), 4n (^{211}Fr 17%), 6n (^{209}Fr 10%), 3n (^{212}Fr 1.0%), and p4n (^{210}Rn 0.7%). Together these channels constitute almost 98% of all fusion reactions cross section. The calculated excitation energy of the CN, at which the fission occurs is $E^\star = 61.0 \pm 6.2$ MeV with the experimental cross sections [23] and $E^\star = 61.7 \pm 6.1$ MeV with the HIVAP cross sections. The same calculations give 49.1 ± 6.1 MeV and 56.9 ± 6.0 MeV for the 4n and 5n channels, respectively. The weighted mean rotational energy for the fission channel was calculated to be $E_{\rm rot} = 4.3 \pm 2.3$ MeV [26]. Using PACE4 [27,28] code we have also calculated the angular momentum distribution of the CN, and the average value, calculated using the same method as for the excitation energy, was found to be $\langle J \rangle = 30 \pm 10\ \hbar$. Due to the sharp decline in the fission cross section the $E^* - J$ space is constrained to a relatively narrow range, as presented in Fig. 1, where the hatched area shows this range within one standard deviation. For the fission process more relevant is the excitation energy above the rotating ground state. As the angular momentum decreases with projectile energy, same is true for the $E_{\rm rot}$, and this effects in even narrower excitation energy range, with its mean value of $\langle E^{*\prime} \rangle = \langle E^* - E_{\rm rot} \rangle = 57.5 \pm 4.8$ MeV. Theoretical fission barrier for $L = 0$ is 14.8 MeV calculated with macroscopic-microscopic model [29], or 7.8 MeV with macroscopic model [26] using the BARFIT subroutine. The latter model allows to include the effects of angular momentum of CN, and weighted barrier height, using the cross sections and angular momentum distribution, was found to be lowered to 5.9 MeV.

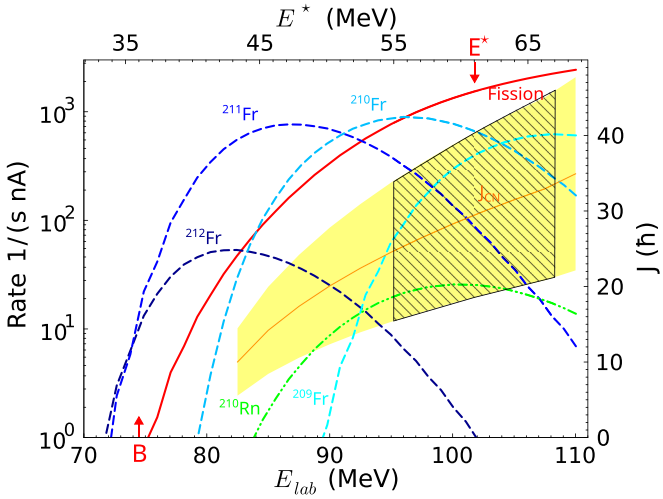

FIG. 1. Reaction rates per s per 1 nA intensity of beam for main reaction channels as calculated by HIVAP [24] as a function of the experimental beam energy range (111–0 MeV). Arrows indicate effective excitation energy of CN for fission events ($E^\star$) and theoretical fusion barrier height (B) [30]. The orange curve shows the average value with the band representing one standard deviation of the total angular momentum of the CN as calculated by the PACE4 code [27,28]. The hatched area shows the position of the CN on the E^*-J space within one standard deviation.

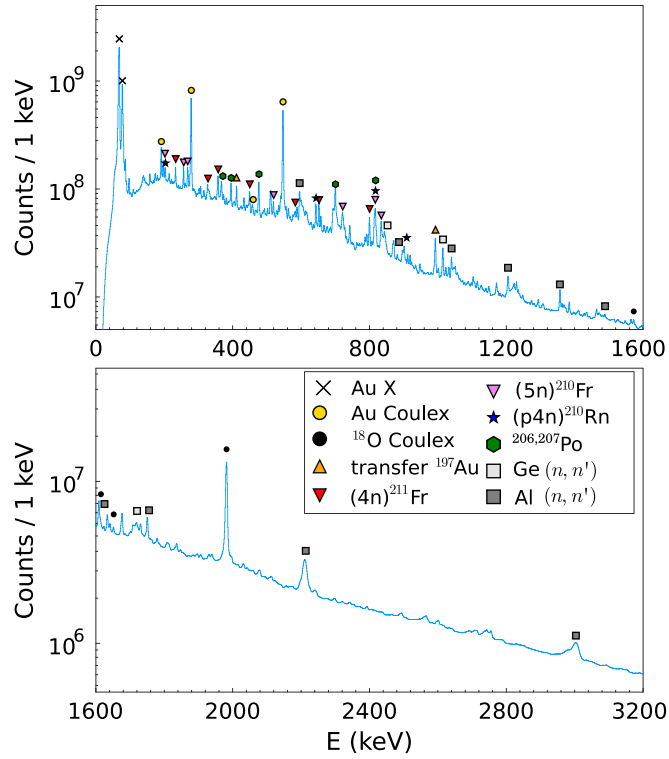

FIG. 2. The total γ ray spectrum from HPGe detectors obtained during the experiment. Some major γ lines are marked with their origin. See text for more details.

Figure 2 presents the total γ spectrum obtained during the experiment. The main contributors to the spectrum are Coulomb excitation of the target (^{197}Au) and projectile (^{18}O), transfer reactions to and from the target (^{196}Pt, ^{198,200}Hg), inelastic neutrons scattering on the detectors and materials (mainly Ge and Al), fusion-evaporation residues (^{210,211}Fr, ^{210}Rn), and their daughter activities (^{206,207}Po). These lines constitute background for the fission reaction. Most intense lines, that have potential for the random coincidences, originate from the Coulomb excitation reaction, but their impact can be reduced by requiring a higher multiplicity ($\geqslant$3 HPGe). Transfer and fusion-evaporation reaction can populate high-spin states and result in the high γ multiplicities, but are less intense, and there is a marginal probability of their random presence in a threefold coincidences. Most care needs to be taken with the (n, n') reactions, which generate true coincidences, as the neutrons are indeed emitted during the fission. However, their characteristic shape and known energies [31], allow their recognition in the fission fragment γ ray spectra.

IV. ANALYSIS

The traditional experimental methods to determine fission yields make use of direct identification of the fragments mass or charge via the TOF/ΔE detectors or spectrometers [7]. An alternative method, based on the detection of the prompt γ radiation from fragments, known already in the 1970s [32] has been recently developed for use with large spectrometers giving promising results [33–38]. This method, used during the first ν-ball campaign at ALTO, was proven very successful at identifying fragments, and giving insight into angular momentum generation [17]. It provides great selectivity, as there is unambiguous fragment identification, and also gives the possibility to extract other information such as γ multiplicity, angular correlations, or total γ energy, which are also of interest. The biggest drawback is, however, its inability to detect small de-excitation branches and direct feeding to the ground state or the first excited state. These factors can potentially introduce systematical errors, and limit the accuracy of the method.

The literature shows a number of examples of fission fragments yields being determined based on the γ spectroscopy. These are almost exclusively limited to the even-even isotopes with well-known low-lying level structure. Methods are based on the detection of the γ rays from the first 2^+ state ($2^+_1 \rightarrow 0^+_{\text{g.s.}}$) [32], coincidence of this transition with the $4^+_1 \rightarrow 2^+_1$ [37] or all possible transitions feeding the 2^+_1 state [34,39]. Other approaches rely on coincidence of the $2^+_1 \rightarrow 0^+_{\text{g.s.}}$ or $4^+_1 \rightarrow 2^+_1 \rightarrow 0^+_{\text{g.s.}}$ with the γ rays emitted by even-even fission fragment partners (i.e., $2^+_1 \rightarrow 0^+_{\text{g.s.}}$ or $4^+_1 \rightarrow 2^+_1 \rightarrow 0^+_{\text{g.s.}}$) [33,36,37], or detection of the $6^+ \rightarrow 4^+_1 \rightarrow 2^+_1 \rightarrow 0^+_{\text{g.s.}}$ cascade [37]. The systematical errors of these methods depend on the type of reaction (e.g., population of the excited levels is different in the spontaneous fission, neutron induced fission, and heavy-ion induced fission), chosen transitions, and quality of the nuclear structure data, including fragments level schemes, level half-lives, etc. Depending on the statistics one can expect the systematical uncertainties to be on the level of 10–30% [33,34,37], typically comparable with the uncertainties associated with the efficiency calibration and statistical errors [34].

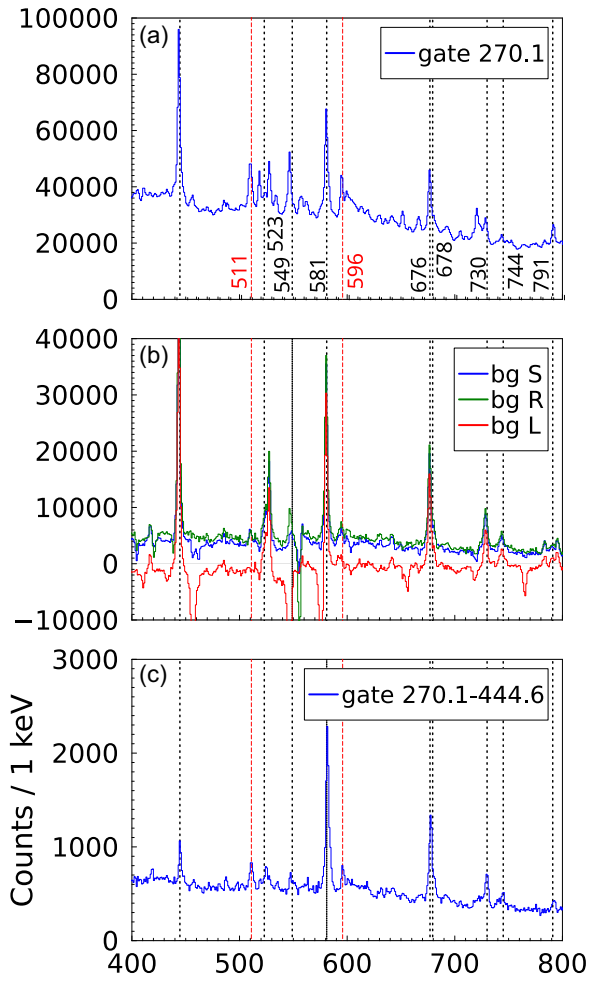

FIG. 3. Example of γ-γ spectrum (top), γ-γ spectrum with background subtraction (middle), and γ-γ-γ spectrum (bottom) gated on the known 270 keV ($2^+ \rightarrow 0^+$) or 445 keV ($4^+ \rightarrow 2^+$) transitions in the ^{106}Ru. Black dashed lines show position of the identified transitions, red dashed lines show the neutron scattering lines and the e^+e^- annihilation line. See text for more details.

The initial system in our study (^{215}Fr) is an odd-Z nuclide, therefore methods based on the correlations between fission fragment γ rays could not be applied. Considerable background coming from reactions other other than fission (cf. Fig. 2) imposed the need to use more selective methods than single or twofold coincidences. Our method is therefore based on threefold γ-γ-γ coincidences using all known transitions leading to the ground state of a given fragment. The selectivity of this method is shown in Fig. 3. γ-γ coincidence spectra (Fig. 3 top) is not sufficient to distinguish between transitions in the ^{106}Ru and in other isotopes (specifically ^{210}Fr which has a γ line at a similar 270 keV energy). Methods based on the γ-γ coincidences with background subtraction, may suffer from the ambiguities arising from the way the background region is selected. The middle panel of the Fig. 3 shows three methods of background subtraction using the gate of the same width as the line gate. These are: symmetric on the both sides of the peak (blue), located to the right (green), and to the left of the peak (red). The intensity or existence of some of the lines may depend on the chosen method. In the γ-γ-γ gate, (Fig. 3 bottom) shown without background subtraction, only the known lines attributed to the ^{106}Ru along with known γ rays originating from the inelastic neutron scattering on the detectors and surrounding material and the $e^+ - e^-$ annihilation line are visible.

The detailed description of the procedure for extraction of the fission fragments yields is given below. We first selected a set of even-even nuclei in the expected region of reaction residuals, i.e., $Z = 26$–64 for fission, and $Z = 78$–86 for transfer, and fusion-evaporation reactions, with N/Z ratio between 1.2 and 1.6 (N/Z for ^{215}Fr is 1.47). For all these nuclei, all cascades in the ENSDF database [40], of three γ rays were selected, under the condition that the transitions are directly connected, and that the last transition is feeding the ground state. For each unique cascade, γ-γ-γ threefold coincidence spectra were extracted from the experimental data, by setting a condition on the two bottom transitions and requiring that the γ rays were emitted within the prompt gate (i.e., ± 15 ns, relative to the beam pulse). Each spectrum was then inspected to search for the third feeding transition.

As an example, Fig. 4 presents results obtained for three nuclides. In ^{106}Ru only the $6_1^+ \rightarrow 4_1^+ \rightarrow 2_1^+ \rightarrow 0_1^+$ cascade is observed. The existence of low-lying 0_2^+ in ^{116}Cd introduces additional fragmentation apart from commonly observed in other nuclei feeding from $5_1^- \rightarrow 4_1^+ \rightarrow \ldots$. Finally, ^{110}Pd shows greatest fragmentation of the observed feeding, where it is spread over 6 levels, and even though the 6_1^+, as expected, is dominant, it yields only 48% of the feeding.

A total of 147 isotopes, 2561 gates, and 13591 lines were analyzed with an automatic fitting procedure. The conditions for accepting a line were: energy within ± 1 keV compared to the value known from database, correct line width ($\sigma = 0.5$–1.5 keV, energy dependent), area of the peak larger than 0 within the 3σ test, and negative result of the Kolmogorov-Smirnov statistical test at 5% confidence level. The latter condition was testing the hypothesis that the distribution of counts within the expected peak area is from the same distribution as the counts area outside of the peak. The results of the automatic procedure were next critically inspected, and in some cases corrected, mostly due to a doublets, nearby line, or a γ ray originating from the (n, n') reaction with energy close to the expected value for the analyzed line.

The intensities obtained were corrected for the half-life of the following isomeric states in the range of 1 ns–1 µs: ^{92}Zr ($6^+/5^-$), ^{106}Pd (5^+), ^{120,122}Sn (5^-), ^{130}Xe (6^+), and ^{138}Ba (6^+). Three longer lived isomeric states above the analyzed cascades were also identified: ^{84}Kr (8^+) 1.83 µs, ^{120,122}Sn (7^-) 11.8 µs, and 7.5 µs. In these cases, the intensities were corrected based on the time gate opened for the whole cycle. Next, we obtained corrections for the β-decay contribution for all the studied isotopes using the coincidences in the delayed window in respect to the beam pulse. The only ambiguity has arisen in the case of ^{120,122}Sn, were the isomeric 7^- states are also populated in the β decay of 8^- isomers of ^{120,122}In. As the ratio of the population of isomers to the ground states in fission is not known, and the states half-lives are substantially longer than the beam pulsing, it is not possible to determine what part of the intensity should be attributed to the β decay.

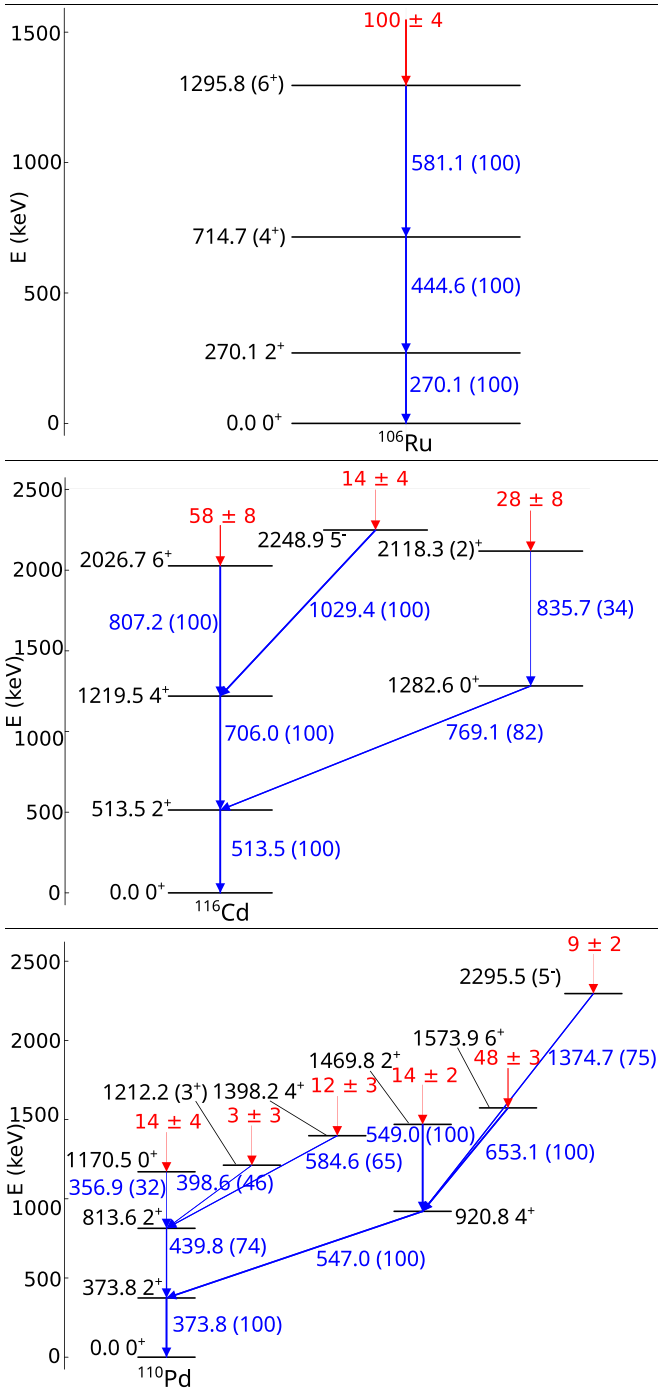

FIG. 4. Example of the observed feeding patterns of fission fragments. Black numbers indicate levels and their spin. Blue values show gamma transitions and their relative intensity in brackets. Red labels and arrow show observed feeding to the indicated state.

Since the population of the high-spin isomers is expected to be smaller than the ground state, in these cases we assumed that the contribution from β decay is negligible, but an additional systematical error may have been introduced here.

Using the information on the transitions absolute intensities we were able to calculate the absolute population of the levels of interest in the fission fragments, and following that, the total fragment population. If cascades were originating from the same initial level, the feeding was calculated as the weighted average of all the cascades starting from the level. In total we found a 144 level feedings in 69 isotopes, including 60 fission fragments. See Supplemental Material [41] for a detailed table with numerical values for observed number of individual fission fragments. The results are discussed in detail in the next section.

One of the main limitations of the spectroscopic method of yield determination lies in the inability to detect the ground state feeding. Using the threefold coincidences based on the transitions in only one of the fission partners, we are also unable to detect the direct feeding to the first and second excited states in the cascade. As it was observed in [37], the population above 4_1^+ level tends to be fragmented, and relaying solely on $6_1^+ \rightarrow 4_1^+ \rightarrow 2_1^+ \rightarrow 0_1^+$ is therefore unreliable. The method presented here overcomes this limitation by analyzing all kinds of transitions, and possible systematic errors are coming only from the direct population of the lowest levels, with events of multiplicity of 2 and less. While this side feeding can be important [17], it results in the systematical errors only if there are significant differences between isotopes. Such effects were observed in the neutron induced fission of ^{238}U [34], and to some extent in the heavy-ion induced fission (^{18}O + ^{208}Pb) [33].

In order to determine the impact of this effect we used a similar method as described before, but based on the γ-γ coincidences for all possible known transitions de-exciting to the ground state. This method is therefore able to detect the direct feeding to the second excited state in a given cascade, and possible differences between the two methods may indicate the aforementioned effect. Unfortunately γ-γ analysis suffers from a worse selectivity then that based on three-folded coincidences, and a lower sensitivity to weak transitions that may be ambiguous to identify. For the fragments clearly identified by the both methods we calculated the ratio of the yields obtained ($r = Y_{\gamma\gamma}/Y_{\gamma\gamma\gamma}$). A statistical t test failed to reject the hypothesis that this ratio is uncorrelated with the mass or charge of the fragments. The mean value of r was found to be 1.0 ± 0.35, while the mean relative statistical uncertainty for both methods was at the level of 25%. As a result we conclude that the possible systematical uncertainty due to the undetected direct feeding to the low lying states is lower than the statistical errors and should not affect the distributions obtained in a considerable way.

By applying the Manchester method [42], we have also calculated the average spins of the individual fragments, by detecting all possible transitions above the states used in the fragment yields determination. In this case the analysis is limited by the available knowledge of the excited states in the fragments. In a number of cases we have found transitions from states with an unknown spin assignment, or with a suggested range or lower limit only. Those states were excluded from the analysis, but it clearly affects the overall picture, due to systematical effects connected with more complete level schemes of some the fragments, e.g., those studied in fission of ^{252}Cf or ^{235}U. The results presented in Fig. 5 show the discrete levels population in individual fragment in the function of their mass. The yield is normalized to 100% for

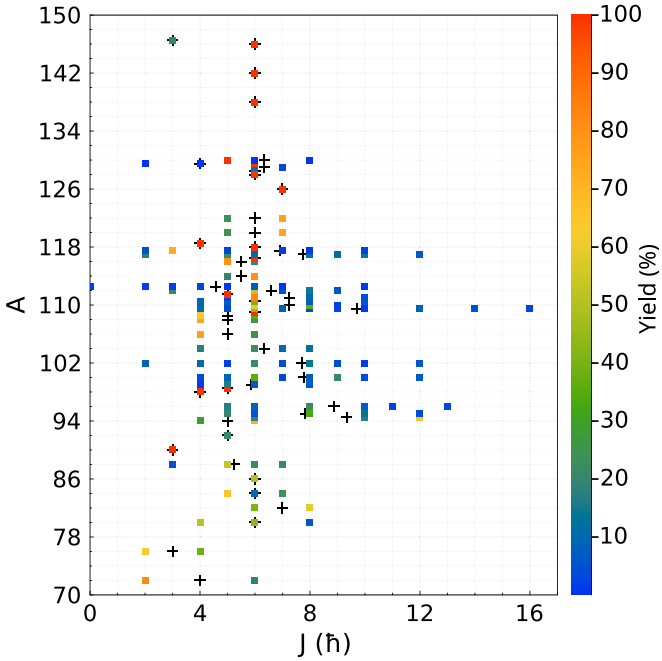

FIG. 5. Individual fragments levels population in function of mass. Crosses show calculated average spin per fragment. Fragments of the same mass are sorted by their charge, and shown next to each other. See text for more details.

each fragment. For the masses with more than one fragment detected, the results are sorted by the fragment charge. The black crosses show the calculated average spin of each fragment. The overall mean spin per fragment was found to be $\bar{J} = 5.9 \pm 1.5\ \hbar$. As a consequence of the aforementioned issues, this result should be treated as a general guidance and qualitative description more than the quantitative value. Our results are close to those described in [42], where a similar reaction was studied (^{19}F + ^{197}Au).

V. DISCUSSION

In order to compare results with theoretical calculations and other experimental results, the yield obtained were normalized so that the sum of observed fragments is equal to 50%. This assumes that there are no systematical differences between even-even, even-odd, and odd fragments, and the impact of nonobserved even-even fragments is negligible. Minimal and maximal observed yields for individual fragments were 0.01(3)% and 3.4(2)% for ^{118}Sn and ^{102}Mo, respectively.

Fragment yields arising from the fission of isotopes in the vicinity of ^{215}Fr were studied previously by measuring the fragments charge [1], these included $^{206–212}$Fr, $^{217–218}$Fr, $^{209–219}$Ra. Fission fragment mass distribution from nearby ^{213}At [43] and ^{214}At [44] were also studied. The francium isotopes were found to breakup in a symmetric way, but $^{214–219}$Ra have a measurable asymmetric component, largest for ^{216}Ra, lying just one proton above ^{215}Fr. The mean position of the heavy fragment in asymmetric fission was shown to be $Z \approx 54$ all across the measured range. Figure 6 shows the charge

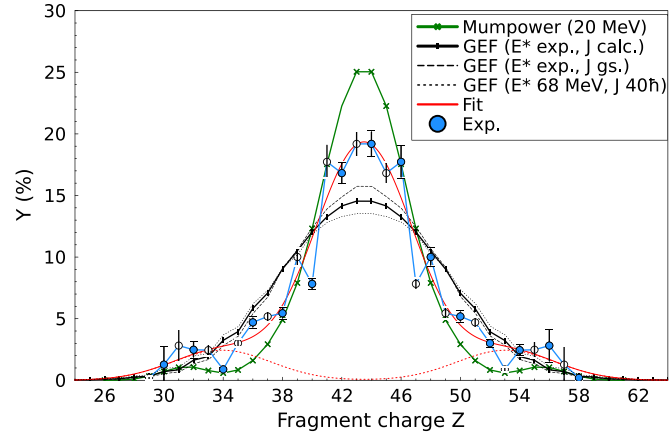

FIG. 6. Experimental and calculated fragment charge distributions (see text for more details).

distribution obtained in our experiment. As the number of protons in the fission is preserved, the experimental points were symmetrized, and yields for the fragments with complementary charge $Z_s = 87 - Z_i$, are shown with the open symbols. This method not only fills in the missing data points for the odd-Z, but presents the self-consistency of the data. Systematical issues with the yield determination method might potentially break the symmetry, which is not observed here.

It is clear that the experimental data cannot be described by a single Gaussian distribution, as on the both sides of the main maximum, there are additional tails, around $Z \approx 54$–56, and $Z \approx 30$–32. Following the procedure described in [1] we fitted a triple Gaussian shape to the experimental distribution using both the unconstrained fit, and a fit with the fixed position for heavy fragment at the $Z_h = 54$ and light at the $Z_l = 33$. Both results are consistent within the uncertainties. The unconstrained fit gives the position of the asymmetric peaks at $Z_h = 53.1 \pm 1.9$ and $Z_l = 33.9 \pm 1.9$. The ratio of symmetric to asymmetric component was found $Y_s/Y_a = 7.6 \pm 1.9$ (6.8 ± 1.1 with the constrained fit). Results of the unconstrained fit are shown in Fig. 6. While these results cannot be directly compared to the systematics in [1], because of a different compound excitation energy and angular momentum, the $Z \approx 54$ asymmetric component is still present, even at such a high excitation energy of $\langle E^{*\prime} \rangle = 57.5 \pm 4.8$ MeV, well above the fission barrier.

Figure 6 presents results obtained with the GEF code [7]. The fission fragments yield was calculated using distribution of energy and angular momentum states of the CN. For each energy step, a FF distribution was calculated for a predicted range of J values. The presented result is a weighted average over excitation energy and J matching the experimental distribution, and PACE4 [27,28] calculations. Distributions calculated for the $L = 0$ (i.e., total angular momentum equal to the ground state), and for $L = 40\hbar$ and $E^* = 68$ MeV are also shown for a reference. The GEF code takes into account angular momentum by modifying fission decay width ([7], Eqs. (85)–(87)), as well as symmetric fission channel width which is calculated based on a modified empirical systematics ([7] Eq. (61)).

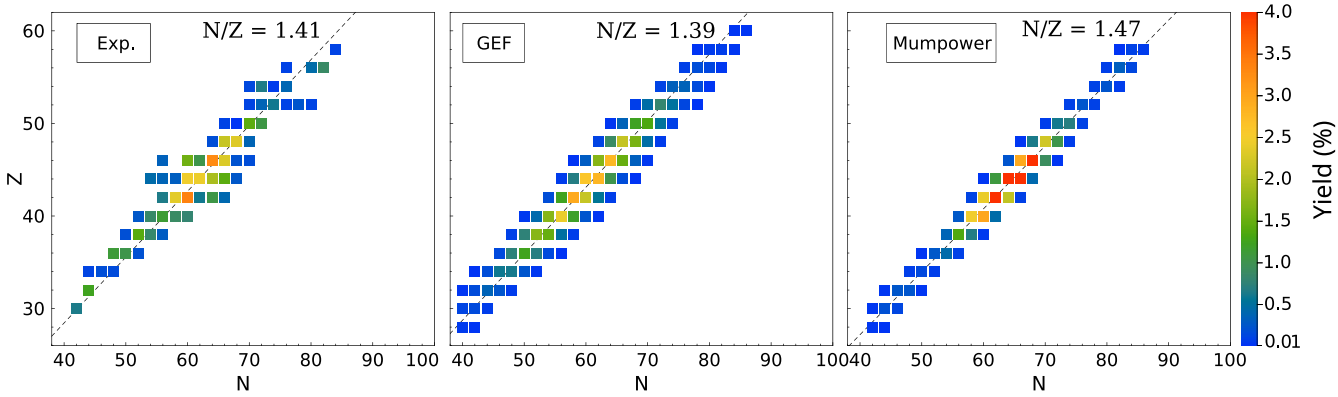

FIG. 7. Left: experimental fragment yield, color encoded. Middle: fragment yield calculated by GEF model [7] for experimental excitation energy and angular momentum. Right: fragment yield calculated by Mumpower *et al.* [11] for excitation energy 20 MeV and $L = 0$. Dashed lines show calculated ratio of N/Z for the given distribution. See text for more details.

For comparison a results of microscopic-macroscopic model by Mumpower *et al.* [11], for which the distribution is available only at an excitation energy slightly above the fission barrier, and ground state J, are also presented. The latter model does not include post-fission de-excitation by the neutron emission, but the charge distribution should be preserved. Both models give the individual isotopic yield, so the experimental data normalization can be verified. By selecting even-even isotopes which are predicted to have yield larger than the experimentally observed minimal value, we obtain the sum of 0.499 for both the GEF and Mumpower models. Due to different excitation energies, the quantitative comparisons are limited, nevertheless the experimental distribution is similar to those predicted by both models. While the GEF predicts a single, wide Gaussian shape (growing wider with an additional angular momentum and energy in the system), the Mumpower model shows a narrower central distribution with the asymmetric components in similar locations to the experimental values, however, with a smaller amplitude.

It is worth noticing that other microscopic models, e.g., [5,45], also show significant asymmetric component in mass distributions for the low energy fission, but lack of charge and full fragments distribution information precludes making detailed comparisons with our data. Nevertheless this fact may indicate that combination of microscopic model, with proper treatment of excitation energy and angular momentum could be sufficient to explain observed distributions. This should include the interplay of increasing probability of energy and angular momentum removal by pre-scission neutrons with excitation energy and J, and a increasing fission barrier height with decreasing spin and possible appearance of asymmetric mode at high E^* and J states.

The method based on γ spectroscopy offers possibility to inspect fragment yields, without losing information due to projections on A or Z directions. This is shown in Fig. 7, where the experimental distribution and those calculated with GEF and by Mumpower models are presented. For clarity the results of the models show only the even-even isotopes with yield above the experimental limit. The dashed lines show the calculated N/Z ratio weighted by the individual yield of the fragments.

The asymmetric component is again seen in the experimental results for $Z = 52$–56, and $Z = 32, 34$. These proton numbers are known to be located around deformed closed shells [1,8,9,46,47]. The mean N/Z ratio for the experimentally observed fragments is 1.41, which indicates on average emission of five neutrons per fission. The results of Mumpower are more confined along N/Z line and shifted to the more neutron-rich side ($N/Z = 1.47$, equal to CN), which is perfectly understandable, as this model predicts only primary fragments, before the neutron emission. The GEF model distribution, which include the neutron emission from the CN and the fragments, is shifted to the left, with $N/Z = 1.39$, which translates to an average of seven neutrons emitted per fission.

The direct comparison of the experimental results with the theoretical models is even more difficult due to the role of the multichance fission. The GEF code predicts a significant contribution of this mode, as only 24% of events are the first-chance fission, and following chances are 14%, 27%, 16%, 15%, and 3% for up to five presaddle neutrons emission respectively, with an average of two pre-fission neutrons emitted. Multichance fission probability is decreasing with increasing angular momentum, but the overall impact is minimal. According to the GEF calculations for the excitation energy $E^* = 66$ MeV, the first-chance fission for $J = 3/2\hbar$ is 17.7%, while for $J = 79/2$ is 18.4%. For the excitation energy $E^* = 52$ MeV, these values are 41.5% and 40.4%, respectively. The details of distribution of excitation energy above rotating ground state, CN angular momentum, and fission barrier height, calculated with GEF [7], PACE4 [27,28], and BARFIT [26] are given in Table I.

The multichance fission mechanism would however inevitably drive the system towards the nuclei which are known to follow the symmetric mode even at low excitation energies, such as $^{212–210}$Fr [1], which cannot be the source of the asymmetric tails. As a result, isotopes $^{213–215}$Fr must have a considerable asymmetric mode contribution even at moderate excitation energies. The multichance fission along with impact of the angular momentum cannot be the only explanation of the observed asymmetric fission mode, as in the case of isotopes of uranium [14]. One must also remember that the GEF

TABLE I. Average values and standard deviations of excitation energy $\langle E^{*'}\rangle$, CN angular momentum $\langle L\rangle$, and fission barrier $\langle B_f\rangle$ for multichance fission channels.

Chance	Prob. (%)	$\langle E^{*'}\rangle$	$\langle L\rangle$	$\langle B_f\rangle$
1	24.2	56.2 ± 5.0	28.7 ± 10.0	5.8
2	14.3	56.6 ± 4.9	29.0 ± 10.0	5.6
3	27.0	57.2 ± 4.8	29.3 ± 9.9	5.5
4	16.5	58.2 ± 4.5	29.9 ± 9.9	5.2
5	14.8	59.8 ± 3.5	30.7 ± 9.7	5.0
6	3.0	60.7 ± 2.9	31.0 ± 9.7	4.8

does not predict a significant role for the asymmetric mode, and overestimates the number of emitted neutrons, which may indicate that the multichance fission impact is lower than that calculated by this model, and origin of the experimentally observed behavior is due to local microscopic effects, beyond statistical and phenomenological approach of the GEF code.

Most of the microscopic model calculations are available at low excitation energy only [5,11,45], and in all cases the authors assume that the asymmetric modes, appearing due to shell effects, should quickly disappear with excitation energy. This statement is common in other approaches, e.g., scission point models [48,49] or microscopic energy density functional model [4,8]. While the disappearance of the asymmetric mode is confirmed by the experimental studies in the heavier nuclei, e.g., ^{226}Th [50] or even slightly lighter, e.g., ^{214}At [44] our observation is on par with observations in the lighter systems, such as isotopes in the sublead region [12,13,51–54], where this mode was shown to be persistent. This might indicate that the disappearance of the asymmetric mode is not universal and neither constrained to the selected regions of the chart of nuclides. This fact is supporting the general connection of the asymmetric mode and deformed shells, and a common mechanism of this mode for both the actinides and the sublead regions [9,55].

VI. SUMMARY

Previously unknown properties of the fissioning system ^{215}Fr at an excitation energy of 61.0 MeV were studied. It was formed as a compound nucleus in ^{18}O and ^{197}Au reaction. Methods based on the spectroscopy of the prompt γ radiation was used to identify the even-even fission fragments. The obtained results may serve as input for planning of the production and spectroscopic studies of a moderately exotic nuclei with heavy-ion induced fission. We have found a significant asymmetric component in the charge distribution, yielding $11.6 \pm 2.9\%$, and located for the heavy fragments around $Z \approx 54$–56. This finding is consistent with a known behavior of nuclei in the actinide region, but rather unexpected at the present excitation energies. The multichance fission mechanism cannot be the only explanation to this phenomena, and ^{215}Fr and neighboring nuclei must have a significant asymmetric mode at moderate excitation energies. There are some conclusions from the microscopic models on the driving force behind asymmetric fission, but dependency on the excitation energy and angular momentum is not fully studied or understood. Our results may call for developments in the description of the fission process as well as new experimental studies which could explore different excitation energies or using neighboring francium isotopes as the fissioning system.

ACKNOWLEDGMENTS

This work was partially funded by the Polish National Science Center under Grant No. 2020/39/B/ST2/02346. This work has been funded by the European Union's Horizon 2020 research and innovation programme Grant Agreement No. 654002 (ENSAR2). Support by Grants No. RTI2018-098868-B-I00 and No. PID2021-126998OB-I00 funded Spanish MCIN/AEI/10.13039/501100011033 and by the European Union is acknowledged.

[1] K.-H. Schmidt, S. Steinhäuser, C. Böckstiegel, A. Grewe, A. Heinz, A. Junghans, J. Benlliure, H.-G. Clerc, M. de Jong, J. Müller, M. Pfützner, and B. Voss, Nucl. Phys. A **665**, 221 (2000).

[2] A. N. Andreyev, J. Elseviers, M. Huyse, P. Van Duppen, S. Antalic, A. Barzakh, N. Bree, T. E. Cocolios, V. F. Comas, J. Diriken, D. Fedorov, V. Fedosseev, S. Franchoo, J. A. Heredia, O. Ivanov, U. Köster, B. A. Marsh, K. Nishio, R. D. Page, N. Patronis *et al.*, Phys. Rev. Lett. **105**, 252502 (2010).

[3] A. V. Andreev, G. G. Adamian, N. V. Antonenko, and A. N. Andreyev, Phys. Rev. C **88**, 047604 (2013).

[4] J. D. McDonnell, W. Nazarewicz, J. A. Sheikh, A. Staszczak, and M. Warda, Phys. Rev. C **90**, 021302(R) (2014).

[5] P. Möller and J. Randrup, Phys. Rev. C **91**, 044316 (2015).

[6] A. V. Andreev, G. G. Adamian, and N. V. Antonenko, Phys. Rev. C **93**, 034620 (2016).

[7] K. H. Schmidt, B. Jurado, C. Amouroux, and C. Schmitt, Nucl. Data Sheets **131**, 107 (2016).

[8] G. Scamps and C. Simenel, Nature (London) **564**, 382 (2018).

[9] G. Scamps and C. Simenel, Phys. Rev. C **100**, 041602(R) (2019).

[10] K. Pomorski, A. Dobrowolski, R. Han, B. Nerlo-Pomorska, M. Warda, Z. Xiao, Y. Chen, L. Liu, and J.-L. Tian, Phys. Rev. C **101**, 064602 (2020).

[11] M. R. Mumpower, P. Jaffke, M. Verriere, and J. Randrup, Phys. Rev. C **101**, 054607 (2020).

[12] K. Nishio, A. N. Andreyev, R. Chapman, X. Derkx, C. E. Düllmann, L. Ghys, F. P. Heßberger, K. Hirose, H. Ikezoe, J. Khuyagbaatar, B. Kindler, B. Lommel, H. Makii, I. Nishinaka, T. Ohtsuki, S. D. Pain, R. Sagaidak, I. Tsekhanovich, M. Venhart, Y. Wakabayashi *et al.*, Phys. Lett. B **748**, 89 (2015).

[13] E. Prasad, D. J. Hinde, M. Dasgupta, D. Y. Jeung, A. C. Berriman, B. M. A. Swinton-Bland, C. Simenel, E. C. Simpson, R. Bernard, E. Williams, K. J. Cook, D. C. Rafferty, C. Sengupta, J. F. Smith, K. Vo-Phuoc, and J. Walshe, Phys. Lett. B **811**, 135941 (2020).

[14] K. Hirose, K. Nishio, S. Tanaka, R. Léguillon, H. Makii, I. Nishinaka, R. Orlandi, K. Tsukada, J. Smallcombe, M. J. Vermeulen, S. Chiba, Y. Aritomo, T. Ohtsuki, K. Nakano, S. Araki, Y. Watanabe, R. Tatsuzawa, N. Takaki, N. Tamura, S. Goto *et al.*, Phys. Rev. Lett. **119**, 222501 (2017).

[15] A. K. Mistry, J. Khuyagbaatar, F. P. Heßberger, D. Ackermann, B. Andel, S. Antalic, M. Block, P. Chhetri, F. Dechery, C. Droese, C. E. Düllmann, F. Giacoppo, J. Hoffmann, O. Kaleja, N. Kurz, M. Laatiaoui, L. Lens, J. Maurer, P. Mosat, J. Piot *et al.*, Nucl. Phys. A **987**, 337 (2019).

[16] M. Lebois, N. Jovančević, J. Wilson, D. Thisse, R. Canavan, and M. Rudigier, Acta Phys. Pol. B **50**, 425 (2019).

[17] J. N. Wilson *et al.*, Nature (London) **590**, 566 (2021).

[18] G. Häfner *et al.*, Phys. Rev. C **103**, 034317 (2021).

[19] Fast acquisition system for nuclear research, http://faster.in2p3.fr.

[20] J. Bezanson, A. Edelman, S. Karpinski, and V. B. Shah, SIAM Rev. **59**, 65 (2017).

[21] The HDF Group, Hierarchical Data Format (1997–2023), https://www.hdfgroup.org/HDF5/.

[22] L. Corradi, B. R. Behera, E. Fioretto, A. Gadea, A. Latina, A. M. Stefanini, S. Szilner, M. Trotta, Y. Wu, S. Beghini, G. Montagnoli, F. Scarlassara, R. N. Sagaidak, S. N. Atutov, B. Mai, G. Stancari, L. Tomassetti, E. Mariotti, A. Khanbekyan, and S. Veronesi, Phys. Rev. C **71**, 014609 (2005).

[23] S. Appannababu, S. Mukherjee, N. L. Singh, P. K. Rath, G. K. Kumar, R. G. Thomas, S. Santra, B. K. Nayak, A. Saxena, R. K. Choudhury, K. S. Golda, A. Jhingan, R. Kumar, P. Sugathan, and H. Singh, Phys. Rev. C **80**, 024603 (2009).

[24] W. Reisdorf and M. Schädel, Z. Phys. A: Hadrons and Nucl. **343**, 47 (1992).

[25] J. F. Ziegler, M. D. Ziegler, and J. P. Biersack, Nucl. Instrum. Methods Phys. Res. B **268**, 1818 (2010).

[26] A. J. Sierk, Phys. Rev. C **33**, 2039 (1986).

[27] A. Gavron, Phys. Rev. C **21**, 230 (1980).

[28] O. B. Tarasov and D. Bazin, Nucl. Instrum. Methods Phys. Res. B **266**, 4657 (2008).

[29] P. Möller, A. J. Sierk, T. Ichikawa, A. Iwamoto, R. Bengtsson, H. Uhrenholt, and S. Åberg, Phys. Rev. C **79**, 064304 (2009).

[30] R. Moustabchir and G. Royer, Nucl. Phys. A **683**, 266 (2001).

[31] M. Baginova, P. Vojtyla, and P. P. Povinec, Appl. Radiat. Isot. **166**, 109422 (2020).

[32] E. Cheifetz, J. B. Wilhelmy, R. C. Jared, and S. G. Thompson, Phys. Rev. C **4**, 1913 (1971).

[33] A. Bogachev, L. Krupa, O. Dorvaux, E. Kozulin, M. Itkis, M. G. Porquet, A. Astier, D. Curien, I. Deloncle, G. Duchene, B. J. P. Gall, F. Hanappe, F. Khalfallah, M. Rousseau, L. Stuttge, N. Redon, and O. Stezowski, Eur. Phys. J. A **34**, 23 (2007).

[34] J. N. Wilson, M. Lebois, L. Qi, P. Amador-Celdran, D. Bleuel, J. A. Briz, R. Carroll, W. Catford, H. De Witte, D. T. Doherty, R. Eloirdi, G. Georgiev, A. Gottardo, A. Goasduff, K. Hadyńska-Klek, K. Hauschild, H. Hess, V. Ingeberg, T. Konstantinopoulos, J. Ljungvall *et al.*, Phys. Rev. Lett. **118**, 222501 (2017).

[35] Studies of Fission Fragment Yields via High-Resolution Gamma-Ray Spectroscopy, EPJ Web Conf. **169** (2018).

[36] B. M. Musangu, A. H. Thibeault, T. H. Richards, E. H. Wang, J. H. Hamilton, C. J. Zachary, J. M. Eldridge, A. V. Ramayya, Y. X. Luo, J. O. Rasmussen, G. M. Ter-Akopian, Y. T. Oganessian, and S. J. Zhu, Phys. Rev. C **101**, 034610 (2020).

[37] A. Dey, D. C. Biswas, A. Chakraborty, S. Mukhopadhyay, A. K. Mondal, L. S. Danu, B. Mukherjee, S. Garg, B. Maheshwari, A. K. Jain, A. Blanc, G. de France, M. Jentschel, U. Köster, S. Leoni, P. Mutti, G. Simpson, T. Soldner, C. A. Ur, and W. Urban, Phys. Rev. C **103**, 044322 (2021).

[38] S. Leoni, C. Michelagnoli, and J. N. Wilson, Riv. Nuovo Cim. **45**, 461 (2022).

[39] P. Banerjee, S. Ganguly, M. K. Pradhan, M. Moin Shaikh, H. P. Sharma, S. Chakraborty, R. Palit, R. G. Pillay, V. Nanal, S. Saha, J. Sethi, and D. C. Biswas, Phys. Rev. C **92**, 024318 (2015).

[40] From ENSDF database as of 12/01/2022 version available at http://www.nndc.bnl.gov/ensarchivals/.

[41] See Supplemental Material at http://link.aps.org/supplemental/10.1103/PhysRevC.108.054608 for a detailed table with numerical values for observed number of individual fission fragments.

[42] Y. Abdelrahman, J. Durell, W. Gelletly, W. Phillips, I. Ahmad, R. Holzmann, R. Janssens, T. Khoo, W. Ma, and M. Drigert, Phys. Lett. B **199**, 504 (1987).

[43] M. G. Itkis, N. A. Kondratiev, S. Mulgin, V. Okolovich, A. Y. Rusanov, and G. Smirenkin, Yad. Fiz. **52**, 944 (1990).

[44] D. Paul, A. Sen, T. K. Ghosh, M. Moin Shaikh, K. Atreya, S. Kundu, K. Banerjee, C. Bhattacharya, S. Bhattacharya, J. K. Meena, D. C. Biswas, B. N. Joshi, N. Kumar, G. K. Prajapati, Y. K. Gupta, K. Mahata, K. Ramachandran, and S. Pal, Phys. Rev. C **102**, 054604 (2020).

[45] L. Ghys, A. N. Andreyev, M. Huyse, P. Van Duppen, S. Sels, B. Andel, S. Antalic, A. Barzakh, L. Capponi, T. E. Cocolios, X. Derkx, H. De Witte, J. Elseviers, D. V. Fedorov, V. N. Fedosseev, F. P. Hessberger, Z. Kalaninová, U. Köster, J. F. W. Lane, V. Liberati *et al.*, Phys. Rev. C **90**, 041301(R) (2014).

[46] W. Nazarewicz, J. Dudek, R. Bengtsson, T. Bengtsson, and I. Ragnarsson, Nucl. Phys. A **435**, 397 (1985).

[47] G. A. Leander, W. Nazarewicz, P. Olanders, I. Ragnarsson, and J. Dudek, Phys. Lett. B **152**, 284 (1985).

[48] N. Carjan, F. A. Ivanyuk, and Y. T. Oganessian, Phys. Rev. C **99**, 064606 (2019).

[49] H. Paşca, A. V. Andreev, G. G. Adamian, and N. V. Antonenko, Phys. Rev. C **107**, 024603 (2023).

[50] A. Y. Rusanov, M. G. Itkis, N. A. Kondratiev, V. V. Pashkevich, I. V. Pokrovsky, V. S. Salamatin, and G. G. Chubarian, Phys. At. Nucl. **71**, 956 (2008).

[51] I. Tsekhanovich, A. N. Andreyev, K. Nishio, D. Denis-Petit, K. Hirose, H. Makii, Z. Matheson, K. Morimoto, K. Morita, W. Nazarewicz, R. Orlandi, J. Sadhukhan, T. Tanaka, M. Vermeulen, and M. Warda, Phys. Lett. B **790**, 583 (2019).

[52] A. A. Bogachev, E. M. Kozulin, G. N. Knyazheva, I. M. Itkis, M. G. Itkis, K. V. Novikov, D. Kumar, T. Banerjee, I. N. Diatlov, M. Cheralu, V. V. Kirakosyan, Y. S. Mukhamejanov, A. N. Pan, I. V. Pchelintsev, R. S. Tikhomirov, I. V. Vorobiev, M. Maiti, R. Prajapat, R. Kumar, G. Sarkar *et al.*, Phys. Rev. C **104**, 024623 (2021).

[53] E. M. Kozulin, G. N. Knyazheva, I. M. Itkis, M. G. Itkis, Y. S. Mukhamejanov, A. A. Bogachev, K. V. Novikov, V. V. Kirakosyan, D. Kumar, T. Banerjee, M. Cheralu, M. Maiti, R. Prajapat, R. Kumar, G. Sarkar, W. H. Trzaska, A. N. Andreyev, I. M. Harca, A. Mitu, and E. Vardaci, Phys. Rev. C **105**, 014607 (2022).

[54] R. Kumar, M. Maiti, A. Pal, S. Santra, P. Kaur, M. Sagwal, A. Singh, P. C. Rout, A. Baishya, R. Gandhi, and T. Santhosh, Phys. Rev. C **107**, 034614 (2023).

[55] T. Ichikawa and P. Möller, Phys. Lett. B **789**, 679 (2019).